Available online at www.sciencedirect.com

ScienceDirect

Ceramics International 40 (2014) 3829–3839

CERAMICS INTERNATIONAL

www.elsevier.com/locate/ceramint

Interactions of high-chromia refractory materials with infiltrating coal slag in the oxidizing atmosphere of a cyclone furnace

Zhijun Zhou, Yu Bo, Yanwei Zhang*, Zhenyu Huang, Le Chen, Lichao Ge, Junhu Zhou, Kefa Cen

State Key Laboratory of Clean Energy Utilization, Zhejiang University, Hangzhou, Zhejiang 310027, People's Republic of China

Received 11 April 2013; received in revised form 4 August 2013; accepted 4 August 2013
Available online 11 August 2013

Abstract

The mechanism of high-chromia refractory failure in the oxidizing atmosphere of cyclone furnaces differs from the reducing atmosphere in gasifiers. In this paper, postmortem analysis was conducted to investigate the changes in the microstructures of exposed high-chromia refractory caused by its interaction with infiltrating coal slag under cyclone furnace conditions. The effects of the temperature level and viscosity of the molten slag were also investigated. Postmortem analysis confirmed that the form of Fe found in the slag in an oxidizing atmosphere was Fe_2O_3 rather than FeO, the phase present in a reducing atmosphere of gasifiers. Furthermore, the higher melting temperature of Fe_2O_3 weakened the slag penetration and chemical corrosion in an oxidizing atmosphere. As coal slag infiltrated a high-chromia refractory, Fe_2O_3 in the slag reacted with Cr_2O_3 until Fe_2O_3 was depleted in the penetrating slag. Cr_2O_3 was dissolved in the slag because of the permeation of the slag in large pores of the refractory. The depth of the slag penetration increased as the temperature increased because of its lower viscosity at higher temperature.

Keywords: B. Failure analysis; C. Corrosion; E. Refractories; Coal slag

1. Introduction

Over the past few decades, coal-water slurry (CWS) has been developed as a substitute for oil in most industries, including power station boilers, gasification technologies, and fluidized bed combustors [1]. The combustion of CWS generally emits less fly ash, SO_2, and NO_x than coal-fired boilers [2]. Slag-tap cyclone furnaces used in clean combustion technology of CWS can substitute for oil and gas combustion systems, and can be used to reduce the emission of fly ash in order to provide clean, high-temperature flue gas for numerous industrial fields.

Similar to coal gasifiers [3,4], slag-tap cyclone furnaces have challenging service conditions, including high temperatures and pressures [5]. During combustion, coal feedstock impurities form a liquid slag when temperatures exceed the melting point of the ash. The molten oxide slag then flows along the surface of the furnace liner, reacting with the refractory at the liner hot-face. Considering the refractories in the combustion chambers are seriously corroded by the molten slag, improving the durability of the refractory materials in it is important. In coal gasification, many refractory compositions are considered or were evaluated as furnace liner materials before the current liner materials were selected. Materials evaluated included sintered or fused cast alumina–silicate, high alumina, chromia–alumina (Cr_2O_3–Al_2O_3), chrome–magnesia, alumina and magnesia, as well as refractories containing SiC and Si_3N_4 [6–8]. Based on laboratory testing [9] and observations after significant service life in gasifiers, refractory materials containing high levels of chrome oxide have been found to have high corrosion resistance against coal slags. They also have the best overall properties for hot-face refractory materials [10]. High-chromia refractory may also be the best choice for a CWS slag-tap cyclone furnace.

Although chromia or chromia–alumina refractory have low solubility in slag and zirconia added in those refractories improves thermal shock resistance, the service life of hot-face Cr_2O_3–Al_2O_3 and Cr_2O_3–Al_2O_3–ZrO_2 compositions in gasifiers is still limited to between 3 months and 36 months [7]. Spalling and slag penetration with chemical corrosion are the primary causes of refractory degradation in a gasifier [11].

*Corresponding author. Tel.: +86 571 87952040; fax: +86 571 87951616.
E-mail address: zhangyw@zju.edu.cn (Y. Zhang).

0272-8842/$ - see front matter © 2013 Elsevier Ltd and Techna Group S.r.l. All rights reserved.
http://dx.doi.org/10.1016/j.ceramint.2013.08.023

Table 1
Properties of CWS for study.

Proximate analysis (wt%, as received basis)				
Moisture	Ash	Volatile matter	Fixed Carbon	Concentration
37.48	7.31	20.50	34.71	65.67
Net calorific value (kJ/kg)			Viscosity (mPa s, 20 °C)	
17238			727.59	
Ultimate analysis (wt%, as received basis)				
C	H	N	S	O
44.26	3.11	0.66	0.43	6.73
Ash fusion point (°C)				
Deformation temperature	Softening temperature	Hemisphere temperature	Flow temperature	
1209	1326	1353	1395	

Besmann [12] conducted thermochemical calculations to simulate the corrosive attack of refractories in slagging gasifiers. Hirata et al. [13] developed an empirical relation for the corrosion rate in these systems. Williford et al. [14,15] explored the application of a volume-shrinkage spalling model to evaluate the material properties of high-chromia refractory and its performance under gasifier operating conditions. Many researchers have thoroughly studied the mechanism of refractory failure based on the postmortem analysis of refractories after significant service life in a gasifier and on laboratory 24-hour slag-refractory cup tests [16–18]. However, few studies have focused on the failure mechanisms of high-chromia refractories used in cyclone furnaces, which may also have similar issues limiting their service life in these applications. In a cyclone furnace, sufficient combustion is required to provide clean high-temperature flue gas for numerous industrial fields. A high air/fuel ratio also can maintain an oxidizing atmosphere, preventing the precipitation of iron in slag from jeopardizing the security of the whole operation. Oxidizing atmosphere [18,19] may induce several other effects on the mechanism of slag-refractory interactions.

In the present study, necessary postmortem analysis were performed to investigate the changes in the microstructures of exposed high-chromia refractory bricks from a pilot-scale cyclone furnace using CWS as fuel. The composition, crystalline phase, microstructures, and porosities of the unused and exposed refractories were analyzed to determine the causes of failure of refractories due to the interaction with the penetrating slag. The effects of temperature and the viscosity of the slag on slag penetration depth were also investigated.

2. Experimental method

The spent refractory liners evaluated in this paper were obtained from a 250 kg/h pilot scale vertical type slag-tap cyclone furnace. The diameter and height of the combustion chamber were 450 and 3000 mm, respectively. CWS was pneumatically injected into the burner from the top of the furnace to mix with the preheated primary air and high-speed tangential secondary air, thus forming an intense swirling motion

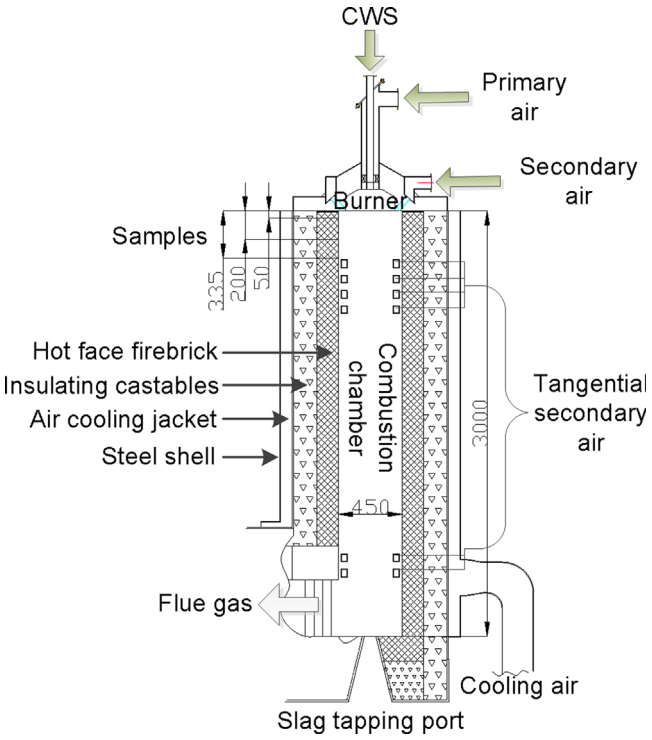

Fig. 1. Schematic of the cyclone furnace refractory structure.

for a high burn-out ratio. The test rig was operated with 100% load and an excess air ratio α=1.4. The excess air ratio was defined as the ratio of the actual air to fuel ratio divided by the stoichiometric air to fuel ratio required for complete combustion. The environment near the hot face refractory was an oxidizing atmosphere. The characteristics of CWS are shown in Table 1. The schematic of the cyclone furnace refractory structure is shown in Fig. 1. High-chromia refractory bricks were used to line the hot face of the furnace, with a castable refractory made of alumina applied as the insulating layer.

The chemical composition of the high-chrome refractory selected for this study and the slag from a continuous slag-tapping port is shown in Table 2. The refractory was removed

after 70 h of operation. Three liner samples were extracted from the location at 50, 200 and 335 mm below the burner. Each sample was cut into 1 cm sections from the slag face to the outer direction radially. Each section was then analyzed for crystalline phase by X-ray diffraction (XRD-D/MAX 2550/PC; Rigaku, Tokyo, Japan). The changes in microstructure were investigated using a scanning electron microscope (SEM-SIRION; FEI, OR), which was carried out at 25 kV. The chemical composition was identified through energy dispersive X-ray (EDX) chemical analysis (SIRON; FEI, OR) at specific points in the slag and in the refractory. The porosity of the samples was measured using a mercury injection instrument (AutoPore IV 9510; Micromeritics, Norcross, GA), with injection pressure from 0.1 psia to 10000 psia (0.68948–68948 kPa). The samples used for pore size determination were crushed to particles with diameter of 5 mm. The viscosity of the slag that was separated from the slag-tapping port was measured using a high temperature viscometer for coal ash (Rheotronic II; Theta Industries, Port Washington, NY) in an oxidizing atmosphere. The viscometer was composed of a Brookfield DVIII ultra programmable rheometer and a high temperature furnace. The furnace temperature control and the data acquisition were obtained through DilaSoft32 software on a computer. The viscometer was calibrated with a standard borosilicate glass, and the measured deviation from the mean was less than 1%. After premelting, 40 g of slag sample was placed in a crucible fixed by a pedestal. The furnace was programmed to heat up from room temperature to about 200 °C above the ash fusion temperature. The heating rate was set to 10 °C/min below 1200 °C and 5 °C/min above 1200 °C. The furnace was left at the target temperature for 30 min in order to stabilize the temperature variations and ensure that the system had reached equilibrium. During that time the spindle was immersed into the molten slag and viscosity measurements taken during stepwise cooling. The rotational speed of the spindle was set from 1 to 15 rpm and adjusted automatically.

Table 2
Chemical composition of high-chromia refractory and slag from slag tapping port.

(Wt%)	High-chromia refractory (apparent porosity = 16.2%)	Slag from slag-tapping port
Unburned carbon	–	0.23
Cr_2O_3	86.37	0.05
Al_2O_3	9.22	30.66
SiO_2	0.19	44.38
ZrO_2	3.74	–
Fe_2O_3	0.051	8.39
CaO	–	7.77
MgO	–	3.66
Na_2O	0.229	3.14
K_2O	–	1.04
TiO_2	0.2	0.68
SUM	100	100

3. Results and discussion

As mentioned previously, the most common causes of refractory failure is chemical corrosion and spalling, although the specific cause of refractory failure varies over time and at

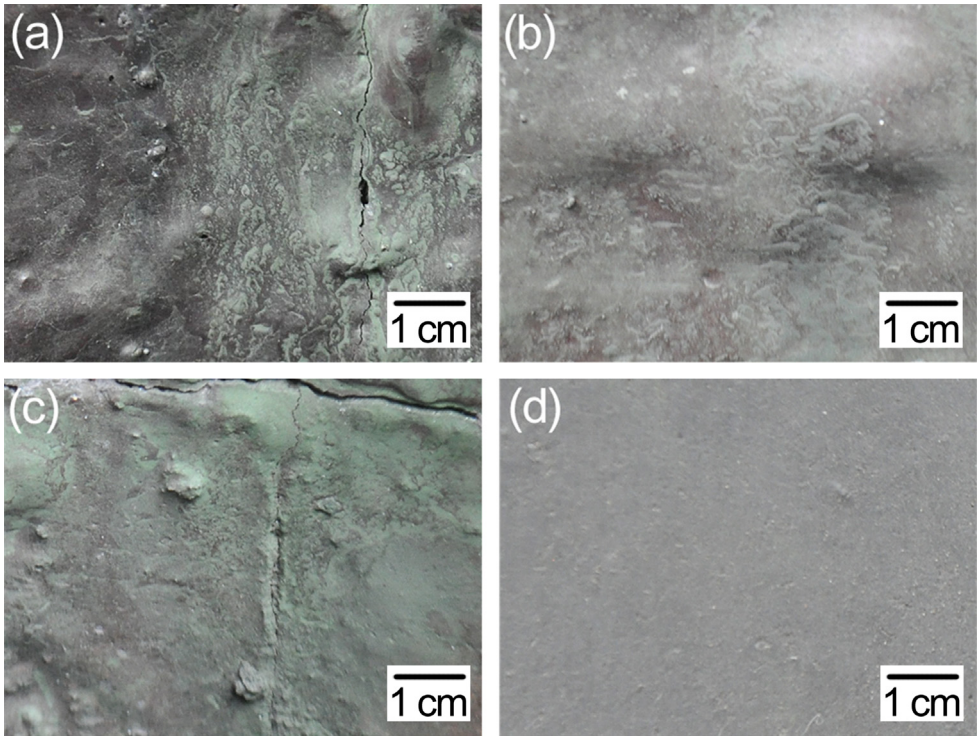

Fig. 2. Hot-face high-chromia refractory viewed from the interior of the cyclone furnace after 70 h of operation: (a) 50 mm, (b) 200 mm, and (c) 335 mm below the burner, (d) unused high-chromia refractory brick.

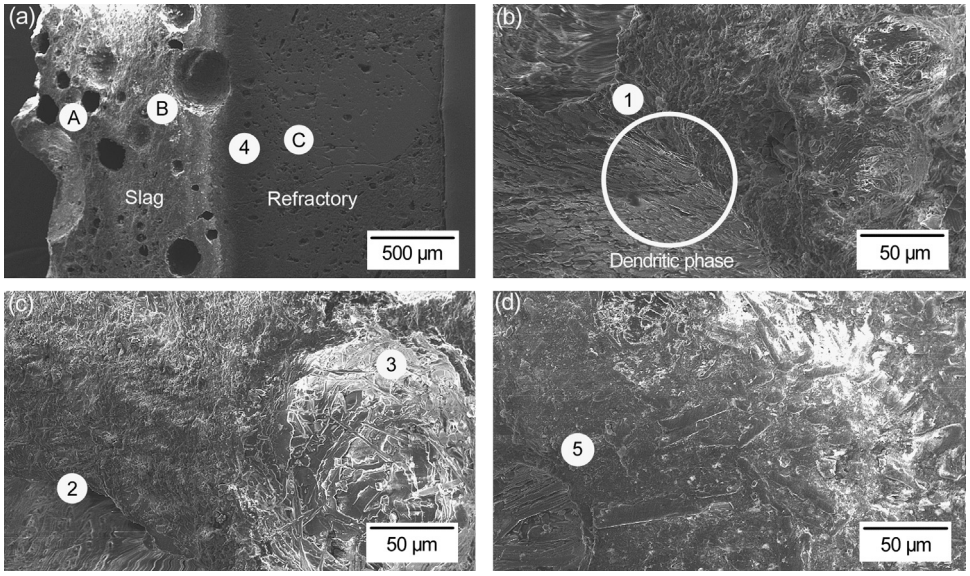

Fig. 3. (a) SEM micrographs of the area at 50 mm below the burner: (b) magnification of A in (a), (c) magnification of B in (a), and (d) magnification of C in (a).

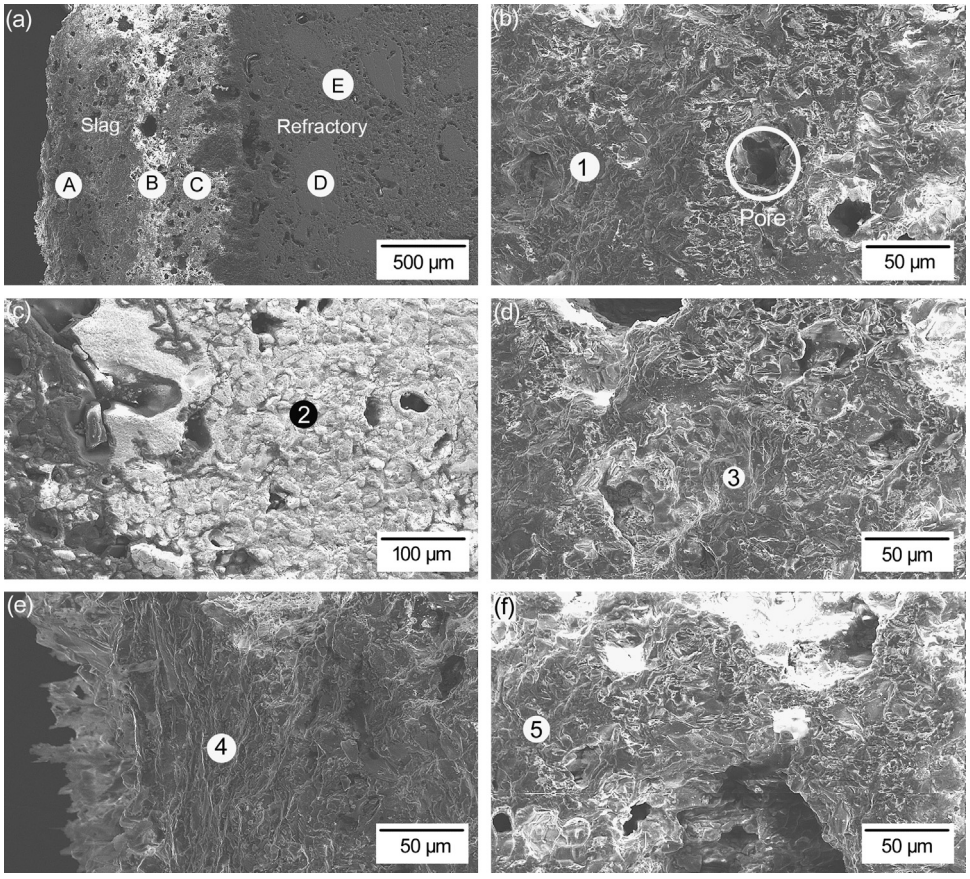

Fig. 4. (a) SEM micrographs of the area at 200 mm from the burner: (b) magnification of A in (a), (c) magnification of B in (a), (d) magnification of C in (a), (e) magnification of D in (a), and (f) magnification of E in (a).

different furnace locations. Fig. 2 shows examples of hot-face high-chromia refractory at 50, 200 and 335 mm below the burner viewed from the interior of the cyclone furnace after 70 h of operation and of an unused high-chromia refractory brick. The main refractory failure at different distances from the burner was dominated by chemical corrosion, which involved the dissolution of refractory material into the slag as it flowed over or penetrated refractory pores. Hot-face

spalling did not occur during the furnace operation (Fig. 2a–c) because of the relatively short exposure time. Compared with the unused high-chromia refractory bricks in Fig. 2(d), the hot-face refractory after the operation was corroded by the molten slag in various degrees. Moreover, the intergranular bond phase was weakened by the corrosion, which led to the removal of refractory grains. However, the overall penetration and corrosion by the slag was not apparent due to the high chemical resistivity and low solubility of chrome oxides in the slag.

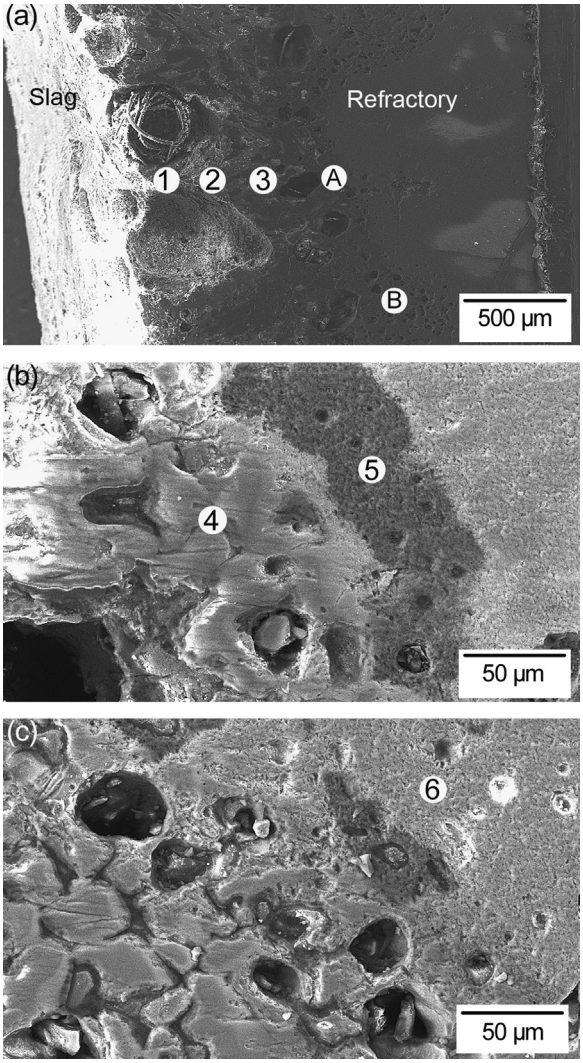

Fig. 5. (a) SEM micrographs of the area at 335 mm from the burner: (b) magnification of A in (a), and (c) magnification of B in (a).

3.1. Microstructure changes in exposed high-chromia refractory bricks

The microstructures of the spent refractory liner were evaluated using samples culled from different locations at 50, 200, and 335 mm below the burner (Figs. 3–5), where the atmosphere was oxidizing. The microstructures by SEM and the composition of used refractory materials by EDX were evaluated as a function of the distance from the burner. All hot face samples had a slag layer remaining on the surface, which can be observed even at 100-fold magnification, as shown in Figs. 3–5.

The representative micrographs of the refractory at 50 mm below the burner are shown in Fig. 3, with the point chemical analysis shown in Table 3. The temperature near the refractory wall at this area was approximately 1300–1330 °C. Fig. 3 shows three layers, i.e., the slag layer, the slag/refractory interface, and the refractory. Large dark-black holes were found in the slag layer, which were air bubbles formed during the cooling of the slag. Meanwhile, relatively small holes were found in the refractory, which were formed during the sintering stage of high-chromia bricks. Area A in Fig. 3(a) is magnified in Fig. 3 (b), showing the slag with an irregular dendritic phase formed during the cooling of the molten slag. The dark slag phase consisted mainly of Na–Al–Si oxides and Mg–Si oxides, which were confirmed by XRD. There was 13.89% Fe in the slag detected at point 1, however, the form of Fe was not determined by XRD because of the presence of many phases of Fe. Fig. 3(c) presents the magnification of area B in Fig. 3(a), which shows the slag area near the slag/refractory interface. This figure shows a similar dark slag phase consisting of Na–Al–Si oxides similar to area A, with nearly the same amount of Fe (12.22%). The bright crystalline phase in area B around a pore showed a low Cr_2O_3 level with clear boundaries on the slag phase background. The presence of Cr_2O_3 indicated the dissolution of Cr_2O_3 in the molten slag during the infiltration. The chemical analysis and crystal phase analysis of point 4 also shows the presence of Ca–Al–Si oxides, Al_2O_3, Cr_2O_3 and Fe_2O_3 at the slag/refractory interface indicated the dissolution of Cr_2O_3 and slag penetration. Area C in Fig. 3(a), magnified in (d) as point 5, showed a dense

Table 3
Chemical analysis of the sample at 50 mm below the burner.

Points	Elements (wt%)									
	Cr	Al	Si	Fe	Ca	Mg	Na	K	Ti	Zr
Point 1	0	16.06	20.08	13.89	6.88	3.26	3.34	1.14	0.75	0
Point 2	0	15.63	18.83	12.22	1.89	3.03	3.16	1.11	0.55	0
Point 3	4.59	16.53	19.41	5.48	5.04	0	0	1.63	0	0
Point 4	19.06	19.24	13.43	2.13	1.78	0	0	0	0	0
Point 5	38.97	12.07	0.17	0.09	0.27	0	0	0	0	3.52

Table 4
Chemical analysis of the sample at 200 mm below the burner.

Points	Elements (wt%)									
	Cr	Al	Si	Fe	Ca	Mg	Na	K	Ti	Zr
Point 1	0.45	15.56	16.21	11.93	6.35	2.28	3.35	1.01	0.68	0
Point 2	3.78	20.51	6.26	7.85	0.7	1.06	3.06	0.56	0.72	0
Point 3	9.32	46.11	0.28	1.03	0.95	0.57	0.48	0.67	0	0
Point 4	55.06	6.73	0	0.94	0.42	0	0	0	0	3.33
Point 5	57.26	6.75	0	0	0	0	0	0	0	3.24

Table 5
Chemical analysis of the sample at 335 mm below the burner.

Points	Elements (wt%)									
	Cr	Al	Si	Fe	Ca	Mg	Na	K	Ti	Zr
Point 1	5.66	14.87	17.38	11.13	6.83	1.85	3.02	1.2	0.11	0
Point 2	7.73	19.91	18.69	8.46	0.69	0.49	2.34	0	0.47	0
Point 3	13.55	15.86	17.03	7.91	0.47	0	2.9	0	0.94	0
Point 4	32.82	8.81	7.17	8.4	3.12	0	1.26	0	0	0
Point 5	40.46	4.14	3.14	5.17	0.16	0	0.06	0	0	2.06
Point 6	71.58	2.34	0.5	0.23	0	0	0	0	0	3.28

phase consisting mainly of Cr, Zr and Al. Little slag composition was detected in this area.

Fig. 4 presents the micrograph of the refractory at 200 mm below the burner with the chemical analysis shown in Table 4. Fig. 4(a) shows the area with slag phases (A), the area full of pores with the same phase (B), the slag/refractory interface (C), and the refractory phases (D, E). The temperature near the refractory wall ranged from approximately 1390–1430 °C, which was near the flow temperature of the CWS ash. Fig. 4 (b) shows the magnification of A in (a) with the dark background as the slag phase containing Na–Al–Si oxides and the dark circular shape as pores. Areas B and C in Fig. 4(a) are magnified in Fig. 4(c) and (d). The slag phases near the slag/refractory interface are the same as those in area A, while the bright layer are fragmented particles containing Cr–Fe–Al oxides with 3.78% Cr, 20.51% Al, and 7.85% Fe (as Fe_2O_3, confirmed by XRD). Point 3 in area C contained primarily Cr and Al, which indicated the depletion of Fe_2O_3 by the reaction between Fe_2O_3 and Cr_2O_3. The fact that Cr–Fe particles aggregated near the slag/refractory interface suggested that Cr_2O_3 dissolved in the slag by chemical corrosion and Fe played a key role in the mechanism of the refractory degradation. The point composition analysis at points 1–5 in Fig. 4 showed similar tendency with those of the other two locations (50 mm and 335 mm from the burner) forming iron oxide spinel (Fe_2O_3), which was confirmed by XRD. Fe_2O_3 then reacted with chromia (Cr_2O_3) at the slag/refractory interface in an oxidizing atmosphere. However, due to the short exposure time and the varying ratio of Fe/Cr, it was difficult to find the peaks by XRD for interaction products $(Cr,Fe)_2O_3$ which probably precipitates out during the cooling. This phenomenon differs from the work reported by Kim et al. [16] that showed in a reducing atmosphere in a gasifier, iron was retained in the FeO state. Under the reducing conditions in the gasifier, the dominant reaction at the slag/refractory interface was that FeO in the slag reacted with Cr_2O_3 in the refractory to form $(Fe,Cr)_3O_4$, which also precipitated during the cooling. Areas D and E in Fig. 4(a) are magnified and shown in Fig. 4(e) and (f), respectively. The continuous dense phase comprised Cr, Al, and Zr oxides. Although area E was less densified because of the pores formed during the curing stage of the high-chromia bricks, both areas D and E were less affected than the slag/refractory interface.

The degradation of the refractory at 335 mm from the burner is shown in Fig. 5 and Table 5, which suggests more infiltration by the molten slag at this area than the first two locations. The slag penetration depth at this area was about 1.5 mm compared with 1.3 and 1 mm at 200 and 50 mm from the burner, respectively. The slag/refractory interface was gradually vaguer as the distance from the burner increased. The gradually increased infiltration was mainly caused by the increase of temperature along the furnace height as the combustion of CWS progressed. The higher temperature (1475–1505 °C) decreased the viscosity of the slag, which reduced the thermodynamic stability of the slag and accelerated refractory corrosion. Fig. 5(b) and (c) present the magnification of areas A and B at the slag/refractory interface near the refractory, respectively. Continuous irregular slag phases consisting of Na–Al–Si oxides with several pores were found (point 1–4), behind which were the dark-grey Cr–Fe–Al

oxides (point 5) with 40.46% Cr, 4.14% Al, and 5.17% Fe (as Fe_2O_3, confirmed by XRD). The well-densified Cr_2O_3 and ZrO_2 phases (point 6) were less affected by the infiltrated slag.

3.2. Crystalline phase analysis by XRD

Each sample used for SEM/EDX analysis was cut into three slices (the slag layer, the slag/refractory layer, and the refractory layer). All the layers were precisely cut based on the results of the SEM/EDX analysis to ensure the reliability of the XRD analysis. The crystalline phases of the samples from different locations at 50, 200, and 335 mm below the burner were analyzed and compared with those of the unused high-chromia refractory sample. As shown in Fig. 6, the unused high-chromia refractory brick in this study contained two crystalline phases. The phases confirmed by XRD were eskolaite(Cr_2O_3) and baddeleyite (ZrO_2).

The XRD patterns of the sample at 50 mm below the burner are shown in Fig. 7. As can be seen, albite ($Na(Si_3Al)O_8$), forsterite ($Mg_2(SiO_4)$), and corundum (Al_2O_3) were found in the slag layer. The slag/refractory interface layer contained anorthite ($Ca(Al_2Si_2O_8)$), corundum (Al_2O_3), hematite (Fe_2O_3), and eskolaite (Cr_2O_3). Anorthite and albite are the crystalline phase commonly observed in the coal slag, which verified the presence of Ca–Al–Si oxides and Na–Al–Si oxides in the SEM/EDX results. No Cr_2O_3 was found in the slag layer, but was found in the slag/refractory layer. Because there was no Cr_2O_3 in the coal ash, all the Cr_2O_3 came from the refractory components. Such result verified the slight degree of the dissolution of Cr_2O_3 in the molten slag. Then, as the depth increased, crystalline phases, such as eskolaite (Cr_2O_3) and baddeleyite (ZrO_2), became dominant in the refractory layer.

Fig. 8 shows the XRD spectrum that reveals albite ($Na(Si_3Al)O_8$), mullite ($Al_{4.68}Si_{1.32}O_{9.66}$), corundum ($Al_2O_3$), and eskolaite ($Cr_2O_3$) in the slag layer of the sample at 200 mm from the burner. As there were no Cr_2O_3 particles in the original coal ash, the higher temperature and lower slag viscosity in this location led to the increased dissolution of Cr_2O_3 identified in the slag layer. The slag/refractory layer contained almost the same phases as the slag layer, while the presence of hematite (Fe_2O_3) and fayalite ($Fe_2(SiO_4)$) indicated the form of Fe in the oxidizing atmosphere was mainly Fe_2O_3.

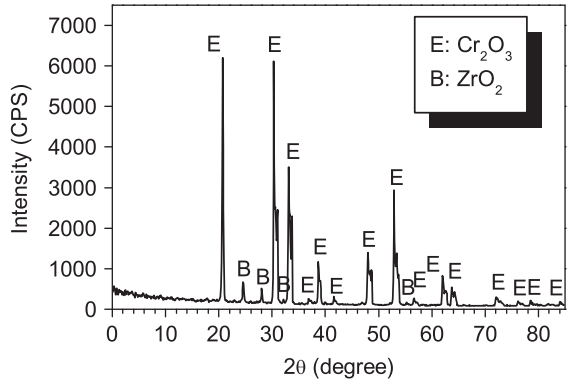

Fig. 6. XRD pattern of the unused high-chromia refractory brick.

The presence of hematite was the initial stage of the reaction between Fe and chromia.

As the temperature increased and the amount of the slag retained on the lining wall decreased, the slag layer and the slag/refractory layer at 335 mm from the burner were difficult to distinguish; thus, the sample was cut into two slices. The XRD patterns of these two slices are shown in Fig. 9. The slag and interface layer contained similar crystalline phases to that of at 200 mm from the burner, but without fayalite ($Fe_2(SiO_4)$). Hematite (Fe_2O_3) was also found in this area. The XRD pattern of all three refractory layer samples in Figs. 7–9 had similar peak positions, i.e., the peak intensities of eskolaite (Cr_2O_3) and baddeleyite (ZrO_2), however, varied due to the heterogeneity of the samples.

Although the crystalline phase detected by XRD analysis was consistent with the change in the microstructure and chemical

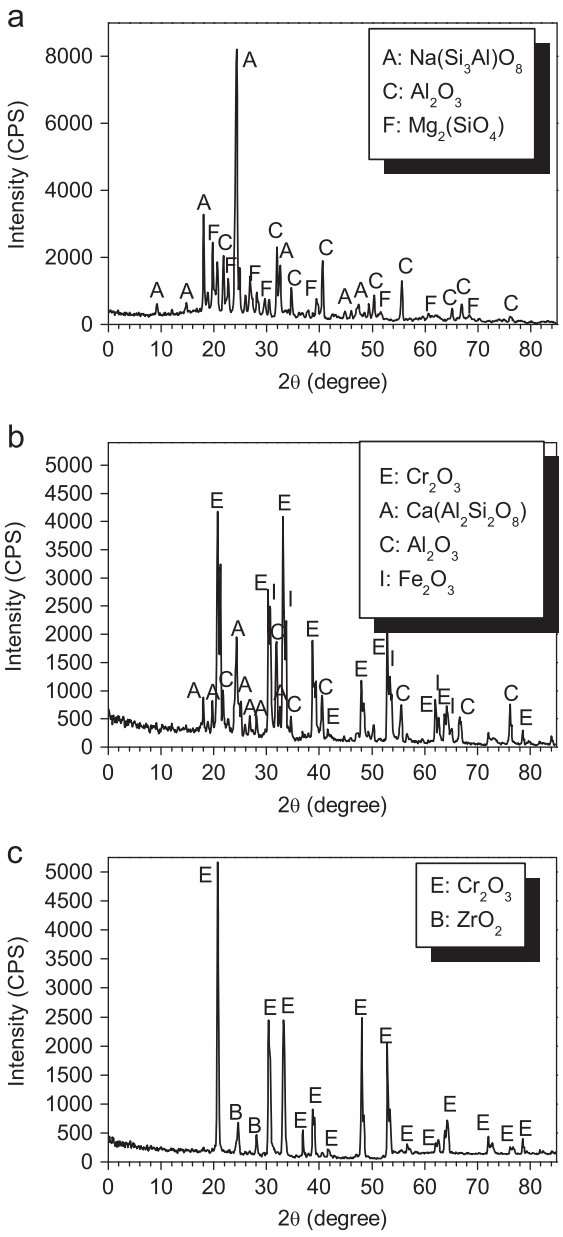

Fig. 7. XRD patterns of the sample at 50 mm below the burner: (a) slag layer, (b) slag/refractory interface, and (c) refractory layer.

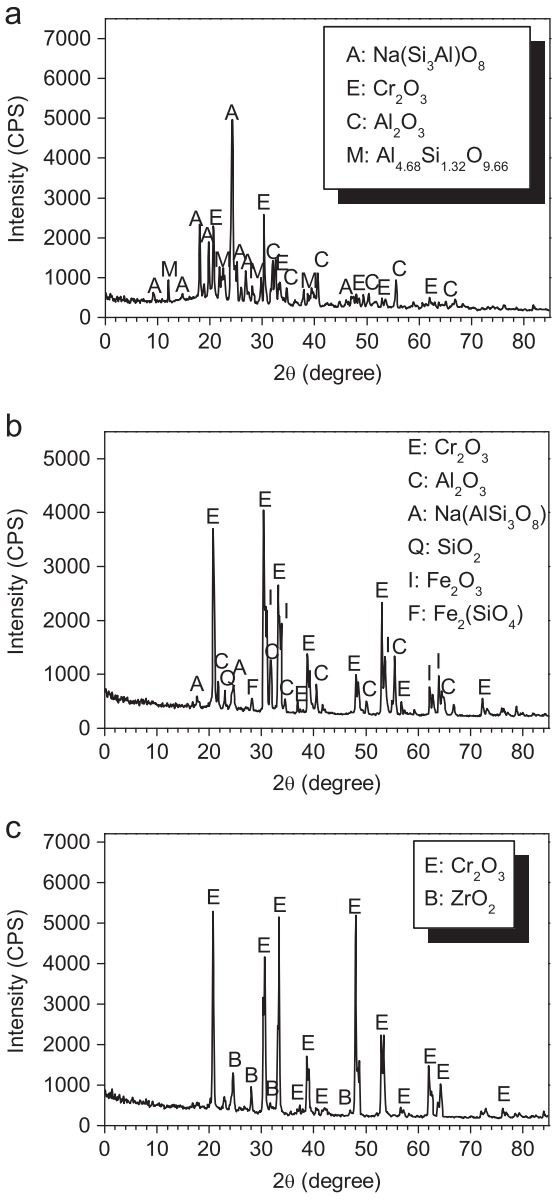

Fig. 8. XRD patterns of the sample at 200 mm below the burner: (a) slag layer, (b) slag/refractory interface, and (c) refractory layer.

composition identified by SEM/EDX, not all microstructure observed using SEM were identified by the XRD analysis, which were present with only the major phases. In this study, the formation of low-temperature melting $Ca(CrO_2)_2$ reported by Rawers et al. [10] was not verified by the XRD analysis, which may be attributed to the difference between the concentration of CaO (7.77% in this study compared with 50% in the synthetic slag in the literature), or because $Ca(CrO_2)_2$ was depleted during the cooling.

3.3. Pore size distribution

In manufacturing high-chromia refractories, corrosion resistance was improved through the use of high-density materials. The high-chromia refractory bricks used in this study had a bulk density of 4.18 g/cm^3. A certain amount of porosity in the refractory bricks (16.2% in Table 6) was necessary due to the thermal gradient and the differential thermal expansion encountered during the heat-up and cool-down, as well as the occasional local thermal excursion that may occur during the operation. Porosity aids in the thermal shock resistance of the refractory, but is also the indirect cause of structural spalling and slag infiltration. The porous nature of chrome oxide refractories and the small thermal gradient near the surface of the brick allows slag to penetrate within the refractory surface, with an average depth of 1.3 mm (as discussed in Section 3.1, the penetration depth was determined by the SEM micrograph according to the scale), resulting in the dissolution of the refractory materials.

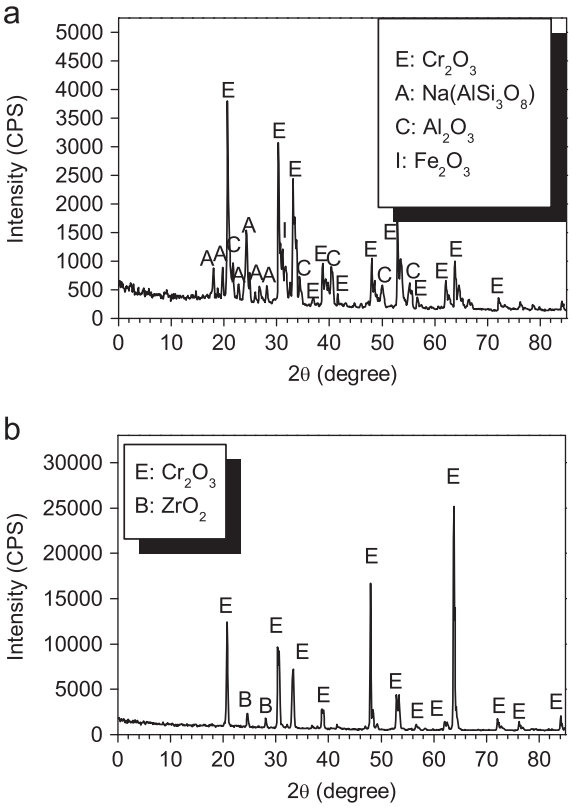

Fig. 9. XRD patterns of the sample at 335 mm below the burner: (a) slag layer and slag/refractory interface and (b) refractory layer.

The pore structure properties of each sample of refractory brick studied in this investigation are provided in Table 6, and the differential curve of the intruded Hg with respect to pore size diameter of the samples from different locations are illustrated in Figs. 10–12. The large amount of porosity (24.2%) of the slag layer sample from 50 mm below the burner indicated that this layer mainly consisted of the residual slag that did not flow along the surface of the liner due to the low temperature in this location (1300–1330 °C). The temperature level, which was much lower than the critical temperature of the slag (1482 °C, as discussed later), caused high slag viscosity (above 160 Pa s) above this temperature. These factors limited the chemical corrosion and slag penetration. Large quantity of pores formed during cooling of the slag caused high slag porosity, surface area, and pore volume, as shown in Figs. 10–12.

Table 6
Pore structure parameters of high-chromia refractory samples.

Sample		Porosity (%)	Total pore area (m^2/g)	Total intrusion volume (mL/g)	Average pore diameter (4 V/A) (nm)
Unused refractory		16.1985	0.009	0.0450	20157.2
50 mm	Slag layer	24.1957	1.490	0.1242	333.5
	Slag/refractory	7.9768	0.153	0.0195	509.0
	Refractory layer	8.2042	0.137	0.0198	576.4
200 mm	Slag layer	7.9963	0.193	0.0212	438.3
	Slag/refractory	9.4142	0.261	0.0229	351.1
	Refractory layer	8.5670	0.270	0.0208	308.8
335 mm	Slag layer	8.4834	0.168	0.0218	518.8
	Refractory layer	8.5371	0.303	0.0206	271.2

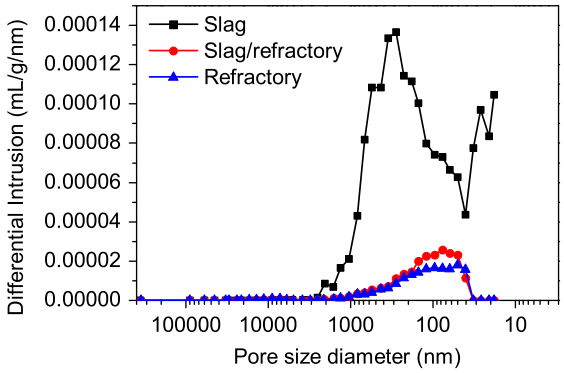

Fig. 10. Pore size distribution of the sample from 50 mm below the burner.

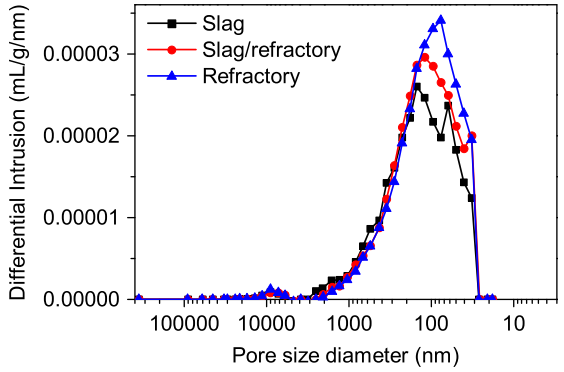

Fig. 11. Pore size distribution of the sample from 200 mm below the burner.

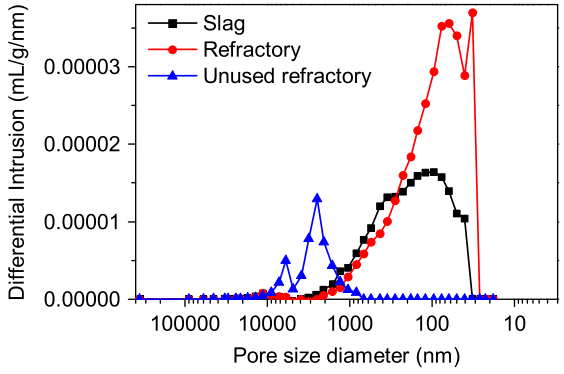

Fig. 12. Pore size distributions of the unused high-chromia refractory and the sample from 335 mm below the burner.

According to results, the average magnitude of the apparent porosity for the other samples of the exposed refractory was approximately 7%–10%. The furnace environments at 200 and 335 mm below the burner had higher temperature levels (1390–1430 °C, 1475–1505 °C, respectively), thus decreasing the viscosity of the molten slag and leading to higher corrosion ability than that of the low temperature areas. As a result, less residual slag remained on the lining wall, and the quantity of pores in the slag was smaller. The porosity of the samples was relatively lower than that of the unused refractory due to the penetration of the molten slag, which permeated the large pores in the refractory brick. As the depth of slag penetration increased, the total pore volume decreased, and was caused by slag infiltration. Meanwhile, the average pore diameter decreased and the total pore area increased because large pores in the refractory brick were replaced by the small pores in the penetrated slag. Combined with the chemistry change, temperature, and viscosity of the slag; low-porosity refractory material with slag in it can prevent further penetration of the slag until the well-densified Cr_2O_3 materials were severely dissolved in the slag.

3.4. Effect of viscosity on slag penetration

Slag penetration is determined by its chemistry, viscosity, and the temperature profile near the refractory, with the viscosity curve measured in the laboratory. The viscosity characteristics shown in Fig. 13 indicated that the critical viscosity of the slag from the slag-tapping port was 44.49 Pa s at the critical temperature of 1482 °C, which was higher than the temperatures at locations of 50 and 200 mm below the burner (1315 and 1410 °C, respectively) but was lower than the temperature at 335 mm below the burner (1490 °C). The critical point of the slag is the temperature where molten slag transits from a plastic state to a real liquid. The viscosity and temperature of this point is defined as the critical viscosity and temperature. However, the slag had certain infiltration and corrosion abilities even though it was not the real liquid phase, because the chemical composition changes also had a great influence on its viscosity.

Fe, Si, Ca, and Al are the most common elements in the slag, and these influence slag penetration into the refractory by changing the viscosity and melting temperature of it [20,21]. As mentioned in Section 3.1, Fe exists in different forms in

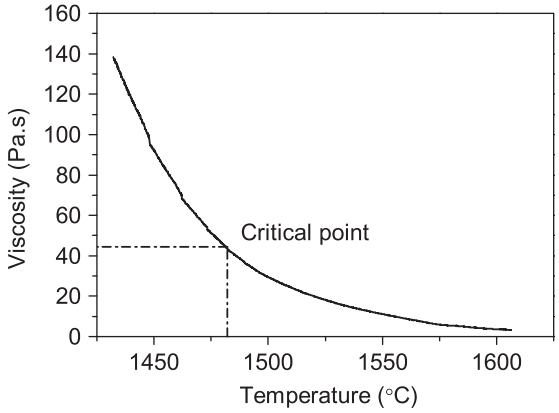

Fig. 13. Viscosity–temperature characteristics of CWS slag from slag-tapping port.

different atmospheres under the combustion and gasification conditions. The $(Fe,Cr)_3O_4$ spinel phase formed in a reducing atmosphere has a melting temperature above 1550 °C; while FeO with lower melting point of 1370 °C caused a lower viscosity slag that interacted with Cr_2O_3 and Al_2O_3 in the refractory grain. The oxidizing atmosphere caused the formation of sesquioxide phases as $(Cr,Fe)_2O_3$ with a high melting point, and with Fe_2O_3, whose melting point is 1595 °C [18]. The high melting temperature of Fe_2O_3 eventually resulted in the higher viscosity, which limited the slag penetration at the combustion temperature.

Combined with the chemistry change discussed in Section 3.1, the depth of the slag penetration increased as temperature increased because of the lower viscosity at higher temperature. Although the slag penetration increased with temperature, it was also limited to a certain extent because the viscosity of the slag increased with the depth of penetration, which can be attributed to the fact that a thermal gradient exists through the hot-face refractory brick [7]. Therefore, along with the short operation time, the refractory of the cyclone furnace was not severely degraded by spalling and chemical corrosion. For the protection of the refractory, the slag with higher viscosity was considered to have a lower ability to corrode the refractory. However, the operation of the slag-tap cyclone furnace required the viscosity of the molten slag to be no more than 50 Pa s, thus the degradation of the refractory during long operation time was inevitable.

Based on the aforementioned analysis and the previously reported work [16], the major difference between the mechanism of slag-refractory interaction in an oxidizing atmosphere and a reducing atmosphere is the existence of Fe, which determines the different reactions during the slag infiltration. In addition, the higher melting temperature of Fe_2O_3 limited the flowing of the slag, thus reducing slag penetration and chemical corrosion in an oxidizing atmosphere.

4. Conclusions

The interaction of the refractory with the infiltrating slag in an oxidizing atmosphere of the cyclone furnace is influenced by the different temperature and viscosity of the molten slag. The oxygen level in the furnace is also critical to the phases formed in slag and slag/refractory interactions. Postmortem analysis confirmed that the existence of Fe in the slag in an oxidizing atmosphere was Fe_2O_3 rather than FeO in a reducing atmosphere. The higher melting temperature of Fe_2O_3 decreased the slag penetration and chemical corrosion in an oxidizing atmosphere. The Cr_2O_3 in the refractory reacted with Fe_2O_3 at the slag/refractory interface before the subsequent depletion of Fe_2O_3. The well-densified Cr_2O_3 and ZrO_2 phases with higher corrosion resistance were less affected by the infiltrated slag. The porosity of the exposed refractory was found to be lower than that of the unused refractory due to the penetration of the molten slag. Such penetration allowed the molten slag to permeate the large pores in the refractory brick to form a slag/refractory interface for the reaction between the slag and the refractory. Finally, the depth of the slag penetration increased as the temperature increased because of the lower viscosity at higher temperature.

Acknowledgment

This research was supported by the National Basic Research Program of China (2012CB214906).

References

[1] T. Wu, M. Gong, E. Lester, F. Wang, Z. Zhou, Z. Yu, Characterisation of residual carbon from entrained-bed coal water slurry gasifiers, Fuel 86 (2007) 972–982.
[2] J.G. Liu, X.M. Jiang, L.S. Zhou, H. Wang, X.X. Han, Co-firing of oil sludge with coal-water slurry in an industrial internal circulating fluidized bed boiler, Journal of Hazardous Materials 167 (2009) 817–823.
[3] X. Cheng, G. Hou, Q. Liang, J. Xu, H. Liu, Experimental study of slag flow on membrane wall in entrained-flow gasifier, Chemical Engineering 40 (2012) 58–62.
[4] J. Rawers, J. Kwong, J. Bennett, Characterizing coal-gasifier slag-refractory interactions, Materials at High Temperatures 16 (1999) 219–222.
[5] D.P. Swoboda, Modifications improve combustion in cyclone boilers, Power Engineering 97 (1993) 44–46.
[6] M.L. Auger, A. Sengupta, V.K. Sarin, Coal slag protection of silicon carbide with chemically vapor deposited mullite coatings, Journal of the American Ceramic Society 83 (2000) 2429–2435.
[7] J.P. Bennett, K.S. Kwong, Failure mechanisms in high chrome oxide gasifier refractories, Metallurgical and Materials Transactions A 42A (2011) 888–904.
[8] P. Biedenkopf, T. Karwath, D. Kobertz, M. Rane, E. Wessel, K. Hilpert, L. Singheiser, Vaporization and corrosion of refractories in the presence of pressurized pulverized coal combustion slag, Journal of the American Ceramic Society 84 (2001) 1445–1452.
[9] T.K. Kaneko, H. Thomas, J.P. Bennett, S. Sridhar, Synthetic coal slag infiltration into varying refractory materials, Journal of the American Ceramic Society 95 (2012) 3325–3333.
[10] J. Rawers, K. Collins, M. Peck, Oxides reactions with a high-chrome sesquioxide refractory, Journal of Materials Science 36 (2001) 4837–4843.
[11] J. Nakano, S. Sridhar, J. Bennett, K.-S. Kwong, T. Moss, Interactions of refractory materials with molten gasifier slags, International Journal of Hydrogen Energy 36 (2011) 4595–4604.
[12] T.M. Besmann, Thermochemical modeling of refractory corrosion in slagging coal gasifiers, CALPHAD: Computer Coupling of Phase Diagrams and Thermochemistry 32 (2008) 466–469.
[13] T. Hirata, T. Morimoto, S. Ohta, N. Uchida, Improvement of the corrosion resistance of alumina-chromia ceramic materials in molten slag, Journal of the European Ceramic Society 23 (2003) 2089–2096.

[14] R.E. Williford, K.I. Johnson, S.K. Sundararn, Modelling of high-chromia refractory spalling in slagging coal gasifiers, Ceramics International 34 (2008) 2085–2089.
[15] R.E. Williford, K.I. Johnson, S.K. Sundaram, S. Pilli, Effective diffusivity and spalling models for slagging coal gasifiers, Journal of the American Ceramic Society 91 (2008) 4016–4022.
[16] H.B. Kim, M.S. Oh, Changes in microstructure of a high chromia refractory due to interaction with infiltrating coal slag in a slagging gasifier environment, Ceramics International 34 (2008) 2107–2116.
[17] K.S. Kwong, J. Bennett, R. Krabbe, H. Thomas, C. Powell, Engineered refractories for slagging gasifiers, American Ceramic Society Bulletin 85 (2006) 17–20.
[18] J. Rawers, L. Iverson, K. Collins, Initial stages of coal slag interaction with high chromia sesquioxide refractories, Journal of Materials Science 37 (2002) 531–538.
[19] L. Molnar, P. Vadasz, M. Kozlovsky, Study of interactions at the slag-basic refractory boundary, Ceramics-Silikaty 37 (1993) 121.
[20] W.J. Song, L.H. Tang, X.D. Zhu, Y.Q. Wu, Z.B. Zhu, S. Koyama, Effect of coal ash composition on ash fusion temperatures, Energy and Fuel 24 (2010) 182–189.
[21] H. Yuan, Q. Liang, H. Liu, X. Gong, Effects of $caco_3$ on the fusion characteristic and viscosity-temperature behaviour of coal ashes, Proceedings of Chinese Society for Electrical Engineering 32 (2012) 49–55.